

Structural and dielectric studies of Mg^{2+} substituted Ni–Zn ferrite

B.B.V.S. VARA PRASAD^{1*}, B. RAJESH BABU², M. SIVA RAM PRASAD¹

¹Department of Physics, MVGR College of Engineering, Chintalavalasa, Vizianagaram, Andhra Pradesh, INDIA-535 005

²Department of Science & Humanities, GVP College of Engineering (W), Madhurawada, Visakhapatnam, Andhra Pradesh, INDIA-530 048

Polycrystalline ferrites having the chemical formula $\text{Ni}_{0.65-x}\text{Zn}_{0.35}\text{Mg}_x\text{Fe}_2\text{O}_4$ ($0 \leq x \leq 0.2$) were prepared by solid state reaction route in steps of $x = 0.04$. The effect of incorporation of diamagnetic divalent magnesium at expense of nickel on the structural properties of these ferrites has been studied. The proposed cation distribution was derived from theoretical X-ray diffraction intensity calculations. These intensity calculations were done by varying the concentration of magnesium ions over two sites in the lattice. For a certain amount of magnesium concentration, the calculated and observed X-ray diffraction intensities were found to be in good agreement. Site occupancy of divalent diamagnetic magnesium was established from this cation distribution. The octahedral environment facilitates magnesium to enter the B-site at about 95 % and the remaining 5 % occupy tetrahedral sites (A-sites). The movements of cations between tetrahedral and octahedral sites as a result of magnesium substitution were discussed in the view of structural parameters, such as tetrahedral and octahedral bond lengths, cation-cation and cation-anion distances, bond angles and hopping lengths, which were calculated using experimental lattice constants and oxygen parameters. All structural parameters showed slight deviations from ideal values. Among all magnesium substituted samples, the ones with $x = 0.12$ exhibited insignificant variation in view of structural properties. Dielectric measurements were conducted at a standard frequency of 1 kHz. Large values of the recorded dielectric constants displayed typical characteristics of bulk ferrites. Both dielectric constant and loss values showed mixed variations, attributed to the loss of zinc ions during the sintering process.

Keywords: *ferrite; magnesium; X-ray diffraction; structure; cation distribution*

© Wrocław University of Technology.

1. Introduction

Ferrites are magnetic ceramics, a mixture of oxides heated at elevated temperatures. These materials have vast applications in electronic and microwave devices [1]. Among several ferrite compositions Ni–Zn ferrites have considerable commercial importance due to their high magnetization and resistivity, low losses and moderate permeability [2, 3]. The structural, electric and magnetic properties not only depend on composition, but also on the distribution of cations/anions over the interstitial sites in the unit cell. The knowledge of cation distribution is vital and it should be well addressed prior to any further investigation. The substitution of any cation into the

parent ferrite system might result in the displacement of other cations between the sublattices, leading to enhancements/deteriorations in properties. These variations can be understood from the site occupancy and charge of the substituted cations. Profound and more comprehensive understanding of these properties with respect to structure facilitates their use in various applications.

Ferrites crystallize into a cubic spinel with a space group $Fd\bar{3}m$, comprising of two sublattices, tetrahedral (A) and octahedral (B) sites. The structure consists of a cubic close-packed array of 32 oxygen ions, which forms 64 tetrahedral vacancies and 32 octahedral vacancies in one unit cell. Every unit cell contains 8 formula units (AB_2O_4). The tetrahedral sites are four-fold coordinated, whereas the octahedral sites are six-fold coordinated by oxygen. Each anion is coordinated by one A-site

*E-mail: varaprasadbbs@gmail.com

and three B-sites. The cation to anion ratio in an ideal spinel structure is 3:4. The distribution of cations over A and B sites can vary from normal to inverse spinel. The formula can be written as $(M_{\delta}^{2+}M_{1-\delta}^{3+}) [M_{1-\delta}^{2+}M_{1+\delta}^{3+}] O_4$, where cations in () brackets show cations at A site and cations in [] brackets show cations at B site. The value of inversion parameter δ gives the nature of the spinel; if $\delta = 1$ it corresponds to the normal spinel structure and for $\delta = 0$ it corresponds to inverse spinel structure.

Several researchers thoroughly investigated magnesium containing ferrite compositions [4, 5]. The site occupancy of magnesium was also discussed to some extent, but the exact amount of magnesium occupancy has not been well investigated in terms of complete structural parameters. In addition, dielectric properties of magnesium substituted Ni-Zn ferrite have not been thoroughly examined. In the present work, light is thrown on magnesium site occupancy and cation distribution is derived from X-ray diffraction data. Furthermore, the effects of diamagnetic divalent magnesium substitution on the structural parameters are discussed on the basis of cation distribution. In addition, dielectric properties are presented and discussed in brief.

2. Experimental

All samples were prepared by double sintering solid state reaction route. The X-ray patterns of all samples confirmed the single phase cubic spinel structure. The preparation method, sintering conditions and characterization were presented in the literature [6]. The X-ray diffraction patterns of all samples are shown in Fig. 1.

After sintering process and prior to the measurements, the surfaces of sintered samples were polished to remove any oxide layer formed during sintering process, which would affect the conducting properties of the samples. The so obtained pellets were of 5 mm thickness and 15 mm in diameter. The polished flat surfaces of the samples were coated with a conducting air-drying silver paint and placed in an oven at 100 °C for about 30 minutes to ensure good ohmic contacts

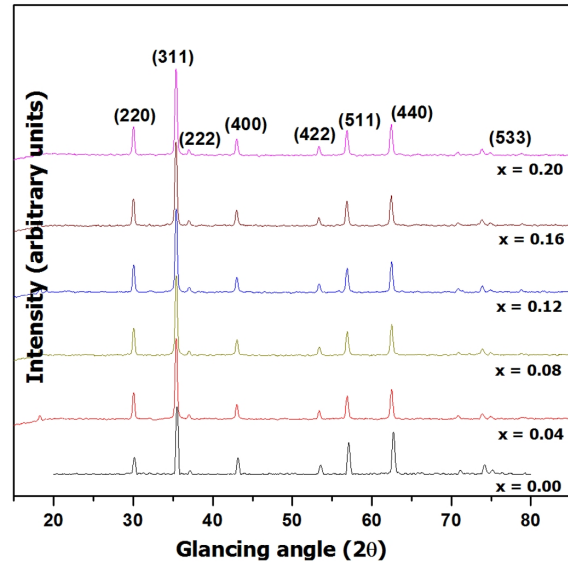


Fig. 1. X-ray diffraction pattern of $Ni_{0.65-x}Zn_{0.35}Mg_xFe_2O_4$ ($0 \leq x \leq 0.2$) in steps of $x = 0.04$.

for two-probe method. Dielectric studies of the samples were carried out by using LCR-Q-METER-SORTER (APLAB model 4912) at 1 KHz frequency and at room temperature. If C is the capacitance, d and A are thickness and surface area of the sample, then dielectric constant:

$$\epsilon' = Cd/\epsilon_0 A \quad (1)$$

where ϵ_0 is the permittivity of air.

The dielectric loss tangent $\tan\delta$ has been calculated from the relation:

$$\epsilon'' = \epsilon' \tan \delta \quad (2)$$

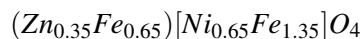
where ϵ'' is the dielectric loss.

3. Results and discussion

3.1. Cation distribution

The distribution of cations over the tetrahedral and octahedral sites for the present ferrite system was derived from the X-ray diffraction data, using the method which is described below. On account of the excellent contrast in atomic scattering factors of substituted Mg^{2+} ions to that of replaced Ni^{2+} ions, the cation distribution from the X-ray diffraction intensities gives a reliable amount

of occupancy of Mg^{2+} ions over the tetrahedral (A-site) and octahedral (B-site) sites. The cation distribution was given for the basic sample on the basis of tetrahedral occupancy of Zn^{2+} [7] and octahedral occupancy of Ni^{2+} ions [8]. Intensity calculations were performed for this distribution and a good agreement between the calculated and observed values has been achieved. The cation distribution for the basic sample is shown below.



In the available literature [9, 11], it was reported that magnesium has a strong preference for octahedral sites, thus, in case of magnesium substituted samples strong octahedral preference of magnesium is taken into account. Intensity ratios were calculated for all magnesium substituted compositions by varying the concentration of magnesium over tetrahedral and octahedral sites, i.e. up to 50 % in either site in steps of 5 %. The cation distribution with the least R-factor was considered as the best.

While calculating theoretical intensities among all observed reflections in the X-ray diffraction patterns, (2 2 0), (4 0 0), (4 2 2) and (4 4 0) planes were considered as suitable for intensity calculations, since these are considered to be structure sensitive planes. Peaks (2 2 0) and (4 2 2) are sensitive to cations on A-site, while (4 0 0) and (4 4 0) are sensitive to cations on both sites [8, 9]. Among all available diffraction peaks, the intensity of (3 1 1) peak was taken as 100 % since the (3 1 1) peak is nearly independent of the oxygen parameter and does not change significantly with cation distribution [10]. At the end, intensity ratios of the selected reflections and the differences (R-factor) were calculated.

The intensity of a diffraction peak (h k l) was calculated from the following formula suggested by Buerger [12]:

$$I_{(hkl)} = |F_{hkl}|^2 p L_P \quad (3)$$

where I_{hkl} is the relative integrated intensity, F_{hkl} is the structure factor, p is the multiplicity factor and L_P is the Lorentz polarization factor, which is given by, $L_P = [(1 + \cos^2\theta) / \sin 2\theta \cos\theta]$.

During calculations of theoretical X-ray diffraction intensities, the temperature factor and the Debye factors are neglected while taking the ratios of intensities [13]. Moreover, the ratios of intensities are not affected by the orientations of the sample, thus, it is justified to consider the intensity ratios rather than individual intensities [14]. Structure factors are calculated by using the following equations [13]:

$$F_{220} = 8F_a \quad (4)$$

$$F_{311} = 2(4F_a + 4\sqrt{2}F_b) \quad (5)$$

$$F_{400} = (8F_a - 16F_b - 32F_o) \quad (6)$$

$$F_{440} = (8F_a + 16F_b + 32F_o) \quad (7)$$

$$F_{422} = -8F_a \quad (8)$$

where F_A , F_B and F_o are structure factors of A-site, B-site cation and oxygen atoms. The structure factor 'F', in an analogy with atomic scattering factors, is defined as a ratio of amplitude of the wave scattered by all atoms to the amplitude scattered by free electrons for the same incident beam. The intensities of the beam diffracted from the crystal depend on the group of atoms in the unit cell and scattering power of these atoms [15].

The best possible cations distribution is chosen on the basis of minimum value of R factor:

$$R = \left| \left[\frac{(I_{hkl})_{cal}}{(I_{h'k'l'})_{cal}} \right] - \left[\frac{(I_{hkl})_{obs}}{(I_{h'k'l'})_{obs}} \right] \right| \quad (9)$$

Among all intensity ratios, three were found to be in good agreement. From these intensity ratios, for the cation distribution with 5 % of magnesium at tetrahedral sites and 95 % of magnesium at octahedral sites, the R factor achieved the minimum value. The difference in the calculated and observed intensities is due to the atomic scattering factors, which have been derived from the electron contributions of atoms at rest, i.e. at absolute zero. Since the X ray diffraction patterns were recorded at room temperature, thermal vibrations of atoms

caused them to occupy a larger volume than they would at rest, which made the scattering less pronounced.

Although for all intensity ratios and all compositions minimum R-factors have been achieved, the intensity ratio $I(4\ 0\ 0)/I(2\ 2\ 0)$ showed large R-factor. The reasons are explained on the basis of the following considerations:

- (i) The presence of cations in different oxidation states (formation of Fe²⁺ ions), thus, occurring of different scattering factors which are not taken into account during calculations.
- (ii) Equation 3 is based on the assumption that it is applicable for the specimens having random orientations in space. However, all polycrystalline specimens show preferential orientation of the grains in a higher or lower degree.
- (iii) The method implemented here, assumes an ideally imperfect crystal, however, in practice, the crystal consists of numerous parallel planes which may be nearly perfect and have low refracting power.

The calculated and observed intensities and R-factors are shown in Table 1.

3.2. Structural parameters

Based on the available data, the cation distribution and Fe_{tetra}/Fe_{octa} ratio for each sample are shown in Table 2.

Based on the above Fe_{octa}/Fe_{tetra} ratios, it is evident that more Fe³⁺ ions are moving to octahedral sites with the increase in magnesium concentration at B-site. Owing to the displacement of Fe³⁺ and Mg²⁺ ions between the two sublattices, their ionic radii change in order to adjust for the particular sublattice. Therefore, the movement of the cations may result in the change of mean ionic radii of the sublattices. The change in the mean atomic radii of both tetrahedral (A) and octahedral (B) sublattices, definitely causes deviations in the arrangement of the nearest neighbouring ions and the interactions between them.

The mean radius of the tetrahedral site is given by:

$$r_A = (0.35r_{Zn(A)} + (0.05x)r_{Mg(A)} + (0.65 - 0.05x)r_{Fe(A)}) \quad (10)$$

where $r_{Zn(A)}$, $r_{Fe(A)}$ and $r_{Mg(A)}$, are the radii of zinc (0.6 Å), magnesium (0.57 Å) and iron (0.49 Å) ions in the tetrahedral site, respectively [16].

The mean radius of the octahedral site is given by:

$$r_B = (1/2)[(0.65 - x)r_{Ni(B)} + (0.95x)r_{Mg(B)} + (1.35 + 0.05x)r_{Fe(B)}] \quad (11)$$

where $r_{Ni(B)}$, $r_{Mg(B)}$ and $r_{Fe(B)}$ are the radii of nickel (0.69 Å), magnesium (0.72 Å) and iron (0.645 Å) ions in the octahedral site, respectively [16].

The estimated values of r_A and r_B are plotted against magnesium concentration and the graph is shown in Fig. 2.

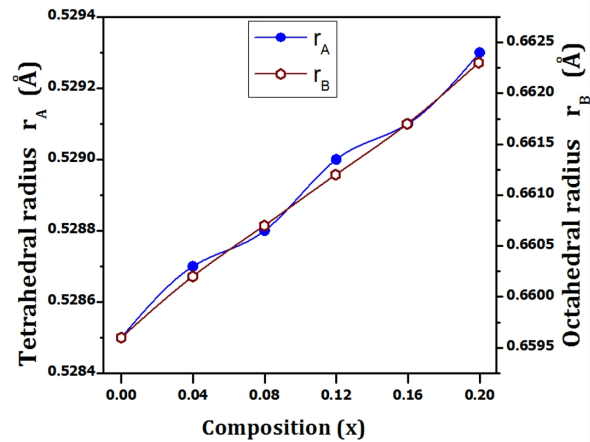


Fig. 2. Mean ionic radii of tetrahedral and octahedral sites (r_A , r_B) of Ni_{0.65-x}Zn_{0.35}Mg_xFe₂O₄ ($0 \leq x \leq 0.2$) in steps of $x = 0.04$.

From the figure, it is clear that there is a slight increase in the mean ionic radius at A-site, since fewer amounts of smaller iron ions are replaced by larger magnesium ions. However, the values of the mean ionic radius at B-site increase noticeably because larger amounts of smaller nickel ions (0.69 Å) are replaced by larger magnesium ions (0.72 Å). Furthermore, smaller amounts of iron

Table 1. Intensity ratios and R-factors of $\text{Ni}_{0.65-x}\text{Zn}_{0.35}\text{Mg}_x\text{Fe}_2\text{O}_4$ ($0 \leq x \leq 0.2$).

Magnesium concentration (x)	A-site	B-site	Percentage of magnesium (%)		I(4 0 0)/I(2 2 0)		I(4 0 0)/I(4 2 2)		I(4 4 0)/I(4 2 2)		I(4 4 0)/I(2 2 0)			
			Calc.	Obs.	R	Calc.	Obs.	R	Calc.	Obs.	R	Calc.	Obs.	R
0 (basic)	-	-	0.9039	1.0067	0.1028	1.0554	0.8730	0.2324	0.8202	0.6355	0.1847	0.8566	0.8022	0.0544
0.04	0	100	0.9042	1.2185	0.3143	0.8657	0.9149	0.0493	0.8197	0.7019	0.1178	0.8562	0.9348	0.0786
	5	95	0.9057	1.2185	0.3129	0.8666	0.9149	0.0484	0.8197	0.7019	0.1177	0.8566	0.9348	0.0782
	10	90	0.9053	1.2185	0.3132	0.8663	0.9149	0.0486	0.8196	0.7019	0.1177	0.8565	0.9348	0.0783
0.08	0	100	0.9045	1.2226	0.3181	0.8658	0.9024	0.0366	0.8198	0.6892	0.1306	0.8564	0.9337	0.0773
	5	95	0.9075	1.2226	0.3151	0.8677	0.9024	0.0348	0.8196	0.6892	0.1305	0.8573	0.9337	0.0764
	10	90	0.9068	1.2226	0.3158	0.8671	0.9024	0.0353	0.8195	0.6892	0.1303	0.8570	0.9337	0.0767
0.12	0	100	0.9105	1.2226	0.3121	0.8695	0.9109	0.0414	0.8198	0.6915	0.1284	0.8584	0.9280	0.0696
	5	95	0.9094	1.2226	0.3132	0.8688	0.9109	0.0421	0.8196	0.6915	0.1282	0.8579	0.9280	0.0701
	10	90	0.9083	1.2226	0.3143	0.8680	0.9109	0.0429	0.8194	0.6915	0.1280	0.8574	0.9280	0.0706
0.16	0	100	0.9051	1.1638	0.2587	0.8662	0.8789	0.0128	0.8199	0.6817	0.1382	0.8568	0.9026	0.0459
	5	95	0.9113	1.1638	0.2525	0.8699	0.8789	0.0090	0.8196	0.6817	0.1380	0.8586	0.9026	0.0440
	10	90	0.9098	1.1638	0.2540	0.8689	0.8789	0.0101	0.8194	0.6817	0.1377	0.8580	0.9026	0.0447
0.2	0	100	0.9051	1.2131	0.3080	0.8662	0.9017	0.0355	0.8205	0.7101	0.1104	0.8574	0.9554	0.0981
	5	95	0.9138	1.2131	0.2994	0.8714	0.9017	0.0302	0.8198	0.7101	0.1096	0.8596	0.9554	0.0958
	10	90	0.9095	1.2131	0.3036	0.8688	0.9017	0.0329	0.8227	0.7101	0.1126	0.8613	0.9554	0.0942

Table 2. Cation distribution and Fe_{tetra}/Fe_{Octa} ratio for different magnesium concentrations (x).

x	Cation distribution	Fe _{Octa} /Fe _{tetra}
0	(Zn _{0.35} Fe _{0.65})[Ni _{0.65} Fe _{1.35}] O ₄	2.0769
0.04	(Zn _{0.35} Mg _{0.002} Fe _{0.648}) [Ni _{0.61} Mg _{0.038} Fe _{1.352}] O ₄	2.0864
0.08	(Zn _{0.35} Mg _{0.004} Fe _{0.646}) [Ni _{0.57} Mg _{0.076} Fe _{1.354}] O ₄	2.0960
0.12	(Zn _{0.35} Mg _{0.006} Fe _{0.644}) [Ni _{0.53} Mg _{0.114} Fe _{1.356}] O ₄	2.1056
0.16	(Zn _{0.35} Mg _{0.008} Fe _{0.642}) [Ni _{0.49} Mg _{0.152} Fe _{1.358}] O ₄	2.1153
0.20	(Zn _{0.35} Mg _{0.01} Fe _{0.64}) [Ni _{0.45} Mg _{0.19} Fe _{1.36}] O ₄	2.1250

ions enter the B-site but the change is not significant. From the values of both r_A and r_B , it is obvious that there may be variation in the lattice constant, but it may not be significant, which is observed in the experimental lattice constant.

Based on the proposed cation distribution, the theoretical lattice constant [17] is calculated using the relation:

$$a_{th} = [8/(3\sqrt{3})][(r_A + R_o) + \sqrt{3}(r_B + R_o)] \quad (12)$$

where R_o is the radius of oxygen ion (1.38 Å).

The substitution of magnesium in the present system of samples may result in expansion/contraction of sublattices, depending on the movement of cations. Thus, the increase in the mean ionic radii of both tetrahedral and octahedral sublattices indicates that there was a slight movement of anions surrounding the cations. The movement of oxygen ions can be explained by means of oxygen positional parameter 'u'. The oxygen positional parameter can be calculated by assuming the origin at A-site or at B-site. Since A-site cation belongs to $\bar{4}3m$ symmetry group, the u parameter, measured by considering the origin at A-site, is denoted by $u_{\bar{4}3m}$. Since, the B-site cation belongs to $\bar{3}m$ symmetry group, the 'u' parameter measured by considering the origin at B-site, is denoted by $u_{\bar{3}m}$.

In the present series of samples, the oxygen positional parameter 'u' has been measured by assuming the centre of symmetry at (3/8, 3/8, 3/8) or origin at A-site ($\bar{4}3m$ symmetry group), also represented as u^{43m} . The oxygen parameter can be calculated from the known r_A and r_B values:

$$r_A = \sqrt{3}a(u - (1/4)) - R_o \quad (13)$$

$$r_B = ((5/8) - u)a - R_o \quad (14)$$

The following formula is used to convert the centre of symmetry from (1/4, 1/4, 1/4) to (3/8, 3/8, 3/8) or vice versa, $u^{43m} = u^{3m} + (1/8)$. The ideal values of $u^{43m} = 0.375$, $u^{3m} = 0.25$.

The values of u^{43m} , u^{3m} as well as experimental and calculated lattice constants are shown in Table 3.

Table 3. Experimental and theoretical lattice constants and oxygen parameter for different magnesium concentration (x).

x	a_{exp} (Å)	a_{th} (Å)	u^{3m}	u^{43m}
0	8.3830	8.3760	0.2564	0.3814
0.04	8.4082	8.3792	0.2561	0.3811
0.08	8.4110	8.3807	0.256	0.3810
0.12	8.4122	8.3823	0.256	0.3810
0.16	8.4155	8.3838	0.256	0.3810
0.2	8.4182	8.3857	0.2559	0.3809

It is obvious from Table 3 that both u values are slightly larger than the ideal values. But the variations are much lower in magnesium substituted samples. The theoretical and experimental lattice constants are in agreement and they show the same trend. The low values of a_{th} are due to the possible formation of Fe²⁺ ions in the samples and the estimation is based on Fe³⁺ ions.

In view of the fact that magnesium is entering both sites at different concentrations, the same as the movement of Fe³⁺ ions, it is quite possible to observe the changes in structural parameters, such as bond lengths, shared and unshared edges, etc.

The inter-ionic distances (bond lengths) at tetrahedral (R_A) and octahedral sites (R_B) were estimated using the following relations [7]:

$$R_A = a\sqrt{3}(\delta + (1/8)) \quad (15)$$

$$R_B = a\sqrt{(3\delta^2 - (\delta/2) + (1/16))} \quad (16)$$

where δ represents the deviation from oxygen parameter, $\delta = u - 0.375$.

The tetrahedral edge length R_x , the shared octahedral length $R_{x'}$ and the unshared octahedral edge $R_{x''}$ of the present ferrites have been calculated using the following equations and they are presented in Table 4:

$$R_x = a\sqrt{2}(2u - 0.5) \quad (17)$$

$$R_{x'} = a\sqrt{2}(1 - 2u) \quad (18)$$

$$R_{x''} = a\sqrt{(4u^2 - 3u + (11/16))} \quad (19)$$

The changes in tetrahedral and octahedral bond lengths are due to the substitution process. The incorporation of magnesium in place of nickel resulted in a small expansion of the tetrahedral site and a prominent expansion of the octahedral site. The expansion of tetrahedral site is observed in terms of mean ionic radius at the tetrahedral site r_A , tetrahedral bond length R_A and shared tetrahedral edge R_x . This expansion of sublattices was attributed to the movement of oxygen ions without changing the structure symmetry. The increase in R_B , $R_{x'}$ and $R_{x''}$ are explained on the basis of oxygen positional parameter 'u'. Since the 'u' value is slightly decreasing with an increase in magnesium concentration, the structure becomes slowly close to an ideal case, oxygen ions are moving towards tetrahedral coordinated cations along $\langle 1\ 1\ 1 \rangle$ direction. This anion dilation happens with the variation in u but this has no effect on the symmetry of the tetrahedra, while the symmetry of octahedra is affected. The change of sublattice symmetries is reflected in bond angles. Since the strength/magnitude of super-exchange interactions is directly proportional to bond angles and

inversely proportional to bond lengths, it is necessary to mention the variations in these parameters with composition. The changes in lattice constant and oxygen parameter can be expressed in terms of cation-cation and cation-anion bond lengths and bond angles.

The cation-cation (Me–Me) and cation-anion (Me–O) bond distances are estimated using the following relations [13]:

Me–Me

$$b = (a/4)\sqrt{2} \quad (20)$$

$$c = (a/8)\sqrt{11} \quad (21)$$

$$d = (a/4)\sqrt{3} \quad (22)$$

$$e = (3a/8)\sqrt{3} \quad (23)$$

$$f = (a/4)\sqrt{6} \quad (24)$$

Me–O

$$p = a((5/8) - u) \quad (25)$$

$$q = a(u - (1/4))\sqrt{3} \quad (26)$$

$$r = a(u - (1/4))\sqrt{11} \quad (27)$$

$$s = a((u/3) + (1/8))\sqrt{3} \quad (28)$$

The estimated values of the bond lengths are shown in Table 5.

From Table 5, a minute increase in cation-cation bond distances from $x = 0$ to $x = 0.2$ is observed. This is a result of larger magnesium incorporation into the octahedral site by replacing smaller nickel, which causes the lattice to expand. Similarly, all anion-cation distances increased due to the expansion of the lattice and little displacement of the oxygen ions. Among all cation-cation bond distances, 'b' values are comparatively small, because there

Table 4. The values of tetrahedral edge length R_x, shared octahedral length R_{x'}, unshared octahedral edge R_{x''}, tetrahedral bond length R_A and octahedral bond length R_B for different magnesium concentrations (x).

x	Shared tetrahedral edge R _x (Å)	Shared octahedral edge R _{x'} (Å)	Unshared octahedral edge R _{x''} (Å)	Tetrahedral bond length R _A (Å)	Octahedral bond length R _B (Å)
0	3.1166	2.8111	2.9658	1.9085	2.0432
0.04	3.1169	2.8286	2.9745	1.9087	2.0524
0.08	3.1171	2.8304	2.9755	1.9088	2.0533
0.12	3.1174	2.8309	2.9759	1.9090	2.0537
0.16	3.1175	2.8331	2.9770	1.9091	2.0548
0.20	3.1179	2.8347	2.9780	1.9093	2.0557

Table 5. The values of (Me–Me) cation-cation and (Me–O) cation-anion bond distances (Å) as a function of magnesium concentration (x).

x	cation-cation bond distances (Å)					cation-anion bond distances (Å)			
	b	c	d	e	f	p	q	r	s
0.00	2.9674	3.4796	3.6343	5.4514	5.1396	2.0454	1.9087	3.6549	3.6648
0.04	2.9727	3.4858	3.6408	5.4612	5.1488	2.0507	1.9092	3.6559	3.6704
0.08	2.9737	3.4870	3.6421	5.4631	5.1507	2.0514	1.9099	3.6572	3.6717
0.12	2.9741	3.4874	3.6425	5.4638	5.1513	2.0508	1.9116	3.6604	3.6726
0.16	2.9752	3.4887	3.6438	5.4657	5.1531	2.0516	1.9123	3.6617	3.6739
0.20	2.9762	3.4899	3.6451	5.4677	5.1550	2.0523	1.9129	3.6630	3.6752

are no intervening anions to obstruct the neighbouring cations.

The angles between these interionic distances (bond angles) were estimated using the simple trigonometric formulae [13]:

$$\theta_1 = \cos^{-1}[(p^2 + q^2 - c^2)/2pq] \quad (29)$$

$$\theta_2 = \cos^{-1}[(p^2 + r^2 - e^2)/2pr] \quad (30)$$

$$\theta_3 = \cos^{-1}[(2p^2 - b^2)/2p^2] \quad (31)$$

$$\theta_4 = \cos^{-1}[(p^2 + s^2 - f^2)/2ps] \quad (32)$$

$$\theta_5 = \cos^{-1}[(r^2 + q^2 - d^2)/2rq] \quad (33)$$

The estimated bond angles are shown in Table 6.

From Table 6, it is clear that there are deviations from the ideal bond angles, observed in all

angles. But the magnesium substitution produced slight variations in the bond angle with the increase in magnesium concentration, showing that there is not much alteration in the alignment of the cations present in the lattice sites. Altogether, the mentioned structural parameters have some slight deviations compared to reported values [7, 18], showing that the magnesium substitution process affected the spinel structure of the present ferrite system. Among all magnesium substituted samples, the composition x = 0.12 showed insignificant variation when compared to successive samples.

3.3. Dielectric studies

In general, ferrites are insulators. But in most of ferrites, conducting nature is observed due to some defects in manufacturing conditions. For instance, sintering in air atmosphere and at high temperatures causes a risk of some cations escape in a form of oxides, which may result in creation of vacancies in interstitial sites of the unit cell. Thus, the

Table 6. The values of bond angles (in degrees) as a function of magnesium concentration (x).

x	θ_1	θ_2	θ_3	θ_4	θ_5
0.00	123.2505	144.5281	93.0037	125.9515	74.2226
0.04	123.3115	144.8055	92.9061	125.9303	74.3952
0.08	123.3096	144.8055	92.9061	125.9303	74.3952
0.12	123.2779	144.6765	92.9578	125.9444	74.3060
0.16	123.2779	144.6665	92.9520	125.9373	74.3060
0.2	123.2779	144.6665	92.9520	125.9444	74.3119

ratio of oxygen anions to the cations may not be equal, which then results in conduction properties.

The observed variations in dielectric constant of ferrites are largely due to space charge polarization which is produced due to the presence of higher conductivity phases (grains) surrounded by the grain boundaries, producing a local accumulation of charges under the influence of an applied electric field. The interfaces could be grain boundaries, intra-granular pores or voids which act as scattering centers for electrons. At lower frequencies, high resistive grain boundaries play a major role, whilst at higher frequencies the conductive grains are more effective [19].

The dielectric behavior of ferrites could be explained on the basis of dielectric polarization in ferrites, which is similar to that of Verwey's conduction mechanism. Many researchers studied and established a strong correlation between conduction mechanism and dielectric constant of ferrites [20]. Ferrites have high dielectric constants at room temperature and at low frequency. The high dielectric constants can also be explained by a close-packed oxygen ion network. Because of the excess charge present on the oxygen ions, it may easily get disturbed by the applied field. Furthermore, in the close-packed network of ions, the number of polarized ions per unit volume is high, especially when Fe^{2+} ions are created. Thus, when electric field 'E' is applied, high polarization is achieved and high dielectric constants are observed as a consequence. In the present series of samples, large dielectric constants have been recorded, which are characteristic of bulk ferrites and they are in match with the reported values of similar ferrite systems [13, 21].

The variation of dielectric constant and loss factor at a frequency 1 kHz is shown in Fig. 3.

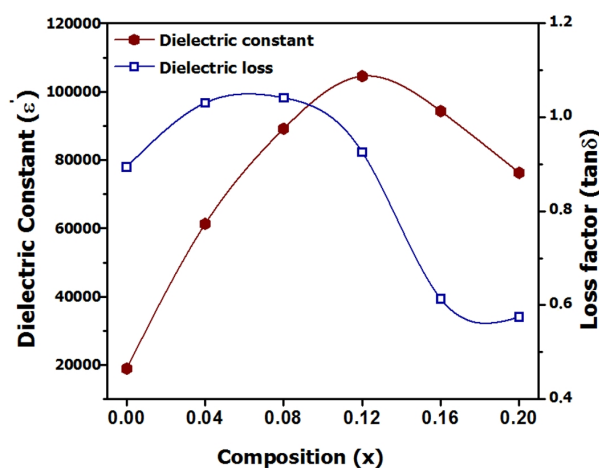


Fig. 3. Dielectric constant and loss factor of $\text{Ni}_{0.65-x}\text{Zn}_{0.35}\text{Mg}_x\text{Fe}_2\text{O}_4$ ($0 \leq x \leq 0.2$) at a frequency of 1 kHz in steps of $x = 0.04$.

The observed variation in the dielectric constant with magnesium concentration could be explained on the basis of local displacement of charge carriers in presence of external electric field and octahedral (B) site occupancy of magnesium ions. In the present system of ferrites, there are two possible conduction mechanisms, electron hopping between $\text{Fe}^{3+} \rightleftharpoons \text{Fe}^{2+}$ as well as hole hopping between Ni^{3+} and Ni^{2+} ions. When nickel containing ferrite systems are sintered and cooled in air atmosphere, a noticeable amount of oxygen is absorbed, giving rise to the formation of Ni^{3+} ions. In oxygen rich region, conduction takes place through $\text{Ni}^{2+} \rightleftharpoons \text{Ni}^{3+}$ mechanism. In oxygen deficient regions, conduction takes place through electron hopping

mechanism between $\text{Fe}^{3+} \rightleftharpoons \text{Fe}^{2+}$. At lower magnesium concentrations (since magnesium is replacing nickel at B-sites), larger number of Fe^{3+} ions are present in B-sites and there is a possibility of electron exchange between $\text{Fe}^{2+} \rightleftharpoons \text{Fe}^{3+}$ due to zinc volatilization [20]. This can also be attributed to the substitution of low resistive magnesium (43.9 nΩ·m) in place of high resistive nickel (69.3 nΩ·m), which decreases the total resistivity or increases the conductivity of the ferrite system. Thus, the charge carriers experience drift caused by the applied field and leading to dielectric polarization, which is clearly displayed in the dielectric constant, especially at $x = 0.12$. At higher magnesium concentrations, the motion of electrons is obstructed by magnesium ions in B-sites and less amount of Ni^{2+} ions available at octahedral sites. Thus, as the electron exchange cannot follow the field causes a decrease of dielectric constant. The increase of hopping length between cations in octahedral sites (b) is also responsible for the decline in dielectric constant. Similar behavior is observed in dielectric loss factor too.

4. Conclusion

Magnesium substituted Ni–Zn ferrite system was prepared by conventional solid state reaction route and the cation distribution was given on the basis of comparing theoretical and experimental intensity ratios. The proposed cation distribution showed that 95 % of magnesium occupy octahedral sites. The magnesium substitution process caused a slight deviation from the spinel structure, which resulted in some changes in structural parameters, such as mean radii of tetrahedral and octahedral sites, bond lengths, shared and unshared edges in the unit cell and bond angles. The dielectric data were explained by dielectric polarization based on electron hopping conduction mechanism at octahedral sites. Dielectric constant increased up to $x = 0.12$ then decreased subsequently. The highest dielectric constant was observed at $x = 0.12$ due to

the presence of Fe^{2+} ions. Dielectric loss also followed the same trend.

References

- [1] HARRIS V.G., *IEEE T. Magn.*, 48 (3) (2012), 1075.
- [2] DIONNE G.F., WEST G.R., *J. Appl. Phys.*, 61 (1987), 3868.
- [3] REZLESCU N., REZLESCU E., PASNICU C., CRAUS M.L., *J. Phys.-Condens. Mat.*, 6, (1994), 5707.
- [4] BERCHMANS L.J., SELVAN R.K., KUMAR P.N.S, AUGUSTIN C.O., *J. Magn. Magn. Mater.*, 279 (2004), 103.
- [5] ROY P.K, BERA J., *J. Magn. Magn. Mater.*, 298 (2006), 38.
- [6] BABU R.B., PRASAD V.B.B.V.S., PRASAD S.M., *Mod. Phys. Lett. B*, 28 (31) (2014), 1450244.
- [7] SMIT J., WIJN H.P.J., *Ferrites*, Philips' Technical Library, Eindhoven, 1959, p. 149.
- [8] LAKHANI V.K, PATHAK T.K., VASOYA N.H., MODI K.B., *Solid State Sci.*, 13 (3), (2011), 539.
- [9] CULLITY B.D., *Elements of X-ray Diffraction*, Addison-Wesley Publishing Company, Massachusetts, 1978.
- [10] WEI Q.-M., LI J.-B., CHEN Y.-J., HAN Y.-S., *Mater. Charact.*, 47 (2001), 247.
- [11] MOHAMMED K.A., AL-RAWAS A.D., GISMELSEED A.M., SELLAJ A., WIDATALLAH H.M., YOUSIF A., ELZAIN M.E., SHONGWE M., *Physica B*, 407, (2012), 795.
- [12] BUERGER M.J., *Crystal Structure Analysis*, Wiley, New York, 1960.
- [13] PRASAD V.B.B.V.S., *Mod. Phys. Lett. B*, 28 (19) (2014), 1450155.
- [14] ZUO Y., LI J., YI J., WANG Z., CHEN C., *J. Solid State Chem.*, 18, (2008), 700.
- [15] DEKKER A.J., *Solid State Physics*, Prentice-Hall Publishers, 1965, p. 15.
- [16] SHANNON R.D., *Acta Crystallogr. A*, 32 (1976), 751.
- [17] SATTAR A.A., EL-SAYED H.M., EL-SHOKROFY K.M., EL-TABEY M.M., *J. Mater. Eng. Perform.*, 14 (2005), 99.
- [18] ABDEEN A.M., *J. Magn. Magn. Mater.*, 185 (1998), 199.
- [19] PRASAD S.R.M., PRASAD B.B.V.S.V., RAJESH B., RAO K.H., RAMESH K.V., *J. Magn. Magn. Mater.*, 323 (16) (2011), 2115.
- [20] EL HITI M.A., *J. Magn. Magn. Mater.*, 192 (1999), 305.
- [21] BATOO K.M., *Physica B*, 406 (3) (2011), 382.

Received 2015-02-02
Accepted 2015-09-22